Entangled-photon generation in nano-to-bulk crossover regime

Motoaki Bamba[1,*] and Hajime Ishihara[2]

[1]*Department of Materials Engineering Science, Osaka University, Toyonaka, Osaka 560-8631, Japan*
[2]*Department of Physics and Electronics, Osaka Prefecture University, Sakai, Osaka 599-8631, Japan*

(Dated: April 23, 2010)

We have theoretically investigated a generation of entangled photons from biexcitons in a semiconductor film with thickness in nano-to-bulk crossover regime. In contrast to the cases of quantum dots and bulk materials, we can highly control the generated state of entangled photons by the design of peculiar energy structure of exciton-photon coupled modes in the thickness range between nanometers and micrometers. Owing to the enhancement of radiative decay rate of excitons at this thickness range, the statistical accuracy of generated photon pairs can be increased beyond the trade-off problem with the signal intensity. Implementing an optical cavity structure, the generation efficiency can be enhanced with keeping the high statistical accuracy.

PACS numbers: 42.65.Lm, 42.50.Nn, 71.35.-y, 71.36.+c

Entangled photons play an important role in quantum information technologies, and the pursuit of high-quality generation of them has become an active research area in the fields of quantum optics and solid-state physics. In addition to the standard method of generating the entangled-photon pairs by using the parametric down-conversion (PDC) in second order nonlinear crystals [1], the generation scheme using a semiconductor quantum dot [2, 3] attracts much attention because we can generate a pure single pair of entangled photons that is highly desired in quantum information processing. On the other hand, the development of entangled photons as an excitation light source is becoming of growing importance for the next-generation technologies of fabrication and chemical reaction [4]. For this purpose, extra high-power and high-quality entangled-photon beams are absolutely necessary. However, any schemes that lead to the generation of such photon beams have not been found yet, although several generation schemes have been investigated so far.

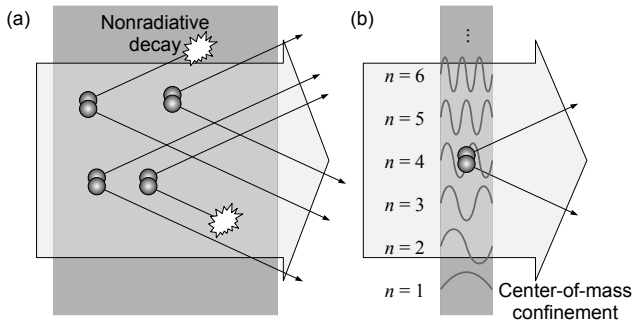

FIG. 1: Sketches of entangled-photon generation from biexcitons (RHPS). (a) In a bulk semiconductor, statistical accuracy worsens by the nonradiative decay of generated photons. (b) In a nano-film, most of photons can go outside by the exciton superradiance, and better accuracy is expected. Center-of-mass motions of excitons and biexcitons are confined in the film.

For the high-power generation of entangled photons, one of the promising candidates is the method involving the biexciton-resonant hyperparametric scattering (RHPS) demonstrated in a CuCl bulk crystal [5, 6]. This generation method is highly efficient owing to the giant two-photon absorption in CuCl crystals [7, 8]. However, as indicated in the experiments [5, 6], we must consider not only the generation efficiency but also the statistical accuracy, i.e., accidentally emitted photon pairs (noise), which come from independent biexcitons and have no entanglement (see Fig. 1(a)). In the scheme for high-power generation of the entangled photons, the amount of entangled pairs (signal) and signal-to-noise (S/N) ratio are always a trade-off, because the nonradiative damping of excitons significantly worsens the S/N ratio of the entangled-photon generation. Although this trade-off problem is seemingly inevitable by the exsistence of the nonradiative damping under the resonant excitation of the elementary excitation in condensed matters, we have revealed that it can be overcome by the enhancement of radiative decay rate of excitons in the crossover regime between the quantum dots and bulk materials [9]. Further, we can also control the characteristics of generated photons by a variety of degrees of freedom in condensed matters and by the peculiar energy structure in the crossover regime [9–11].

Our calculation method is based on the quantum electrodynamics (QED) theory for excitons [12]. Compared to the previous theories [13], we have developed a framework applicable to nanometer and submicrometer films including explicit degrees of freedom of the center-of-mass motion of confined excitons. We consider excitons as pure bosons and introduce an exciton-exciton interaction into the system to discuss the RHPS process. The Hamiltonian of the excitonic system is represented as

$$H_{\rm ex} = \sum_{\mu} \hbar\omega_{\mu} b_{\mu}^{\dagger} b_{\mu} + \frac{1}{2} \sum_{\mu,\nu,\mu',\nu'} V_{\mu,\nu;\mu',\nu'} b_{\mu}^{\dagger} b_{\nu}^{\dagger} b_{\nu'} b_{\mu'}, \quad (1)$$

where b_{μ} is the annihilation operator of an exciton in

state μ, ω_μ is its eigenfrequency, and $V_{\mu,\nu;\mu',\nu'}$ is the nonlinear coefficient. The equation of excitons' motion is derived in ω (frequency) domain as [14]

$$\begin{aligned}&[\hbar\omega_\mu - \hbar\omega - \mathrm{i}\gamma_{\rm ex}/2]\hat{b}_\mu(\omega)\\ &= \int \mathrm{d}\boldsymbol{r}\ \boldsymbol{\mathcal{P}}^*_\mu(\boldsymbol{r})\cdot\hat{\boldsymbol{E}}^+(\boldsymbol{r},\omega) + \hat{\mathcal{D}}_\mu(\omega)\\ &- \sum_{\nu,\mu',\nu'} V_{\mu,\nu;\mu',\nu'}\int_{-\infty}^{\infty}\mathrm{d}t\ \frac{\mathrm{e}^{\mathrm{i}\omega t}}{2\pi} b^\dagger_\nu(t)b_{\nu'}(t)b_{\mu'}(t). \qquad (2)\end{aligned}$$

Here, $\hat{\boldsymbol{E}}^+(\boldsymbol{r},\omega)$ is the positive-frequency Fourier transform of the electric field at position $\boldsymbol{r}$. $\boldsymbol{\mathcal{P}}_\mu(\boldsymbol{r})$ is the coefficient of excitonic polarization $\boldsymbol{P}_{\rm ex}(\boldsymbol{r}) = \sum_\mu \boldsymbol{\mathcal{P}}_\mu(\boldsymbol{r})b_\mu +$ H.c., and is represented as $\boldsymbol{\mathcal{P}}_\mu(\boldsymbol{r}) = \mathbf{M}g_\mu(\boldsymbol{r})$ with the transition dipole moment $\mathbf{M}$ and the exciton center-of-mass wavefunction $g_\mu(\boldsymbol{r})$. $\hat{\mathcal{D}}_\mu(\omega)$ is the fluctuation operator due to the excitonic nonradiative damping with rate $\gamma_{\rm ex}$. The equation of motion of $\hat{\boldsymbol{E}}^+(\boldsymbol{r},\omega)$ is derived as

$$\begin{aligned}&\boldsymbol{\nabla}\times\boldsymbol{\nabla}\times\hat{\boldsymbol{E}}^+(\boldsymbol{r},\omega) - (\omega/c)^2\varepsilon_{\rm bg}(\boldsymbol{r},\omega)\hat{\boldsymbol{E}}^+(\boldsymbol{r},\omega)\\ &= \mathrm{i}\mu_0\omega\hat{\boldsymbol{J}}_0(\boldsymbol{r},\omega) + \mu_0\omega^2\hat{\boldsymbol{P}}^+_{\rm ex}(\boldsymbol{r},\omega), \qquad (3)\end{aligned}$$

where $\varepsilon_{\rm bg}(\boldsymbol{r},\omega)$ is the background dielectric function, μ_0 is the magnetic permeability in vacuum, and $\hat{\boldsymbol{J}}_0(\boldsymbol{r},\omega)$ governs the fluctuation of the electromagnetic fields [12].

The third term on the right-hand side of Eq. (2) is the nonlinear term for the entangled-photon generation, and it is approximately treated as follows. First, we calculate the amplitude $\beta_\mu(\omega) = \langle\hat{b}_\mu(\omega)\rangle$ of excitons in linear regime from Eqs. (2) and (3) by neglecting the nonlinear term and by assuming a pump field as a homogeneous solution of Eq. (3) in classical framework of light. Then, the biexciton amplitude $\mathcal{B}_\lambda(\omega)$ is calculated from $\beta_\mu(\omega)$ and a phenomenologically introduced damping rate $\gamma_{\rm bx}$ of biexcitons [14]. Considering a sufficiently strong pump power compared to the vacuum fluctuation, we can approximately rewrite the nonlinear term in Eq. (2) as $\sum_{\lambda,\nu}(\hbar\omega_\mu + \hbar\omega_\nu - \hbar\Omega_\lambda)F_{\lambda,\mu,\nu}\int_{-\infty}^{\infty}\mathrm{d}\omega'\ b^\dagger_\nu(\omega-\omega')\mathcal{B}_\lambda(\omega')$, where Ω_λ is the eigen frequency of biexcitons in state λ and $F_{\lambda,\mu,\nu}$ is the coefficient giving a biexciton state $|\lambda\rangle = \frac{1}{2}\sum_{\mu,\nu}F_{\lambda,\mu,\nu}b^\dagger_\mu b^\dagger_\nu|0\rangle$. While Ω_λ and $F_{\lambda,\mu,\nu}$ should be determined from Eq. (1), we instead assume them as follows. If the center-of-mass motion of the lowest biexciton level (zero angular momentum) is confined in a crystal sufficiently larger than its Bohr radius, we can approximately express the coefficient as $F_{\lambda,\mu,\nu} = \delta_{\lambda,\mu,\nu}\Phi\int\mathrm{d}\boldsymbol{r}\ G_\lambda(\boldsymbol{r})g^*_\mu(\boldsymbol{r})g^*_\nu(\boldsymbol{r})$, where $|\Phi|^2$ represents the effective volume of relative motion of biexciton, $\delta_{\lambda,\mu,\nu}$ describes the polarization selection rule in the excitation and collapse of biexcitons, and $G_\lambda(\boldsymbol{r})$ is the center-of-mass wavefunction of biexciton state λ.

Under the above approximation, by simultaneously solving Eqs. (2) and (3) up to the lowest order, we evaluate correlation functions of $\hat{\boldsymbol{E}}^+(\boldsymbol{r},\omega)$ from commutation relations of fluctuation operators $\hat{\mathcal{D}}_\mu(\omega)$ and $\hat{\boldsymbol{J}}_0(\boldsymbol{r},\omega)$ [12]. The scattering intensity is evaluated by the first-order correlation $C^{(1)}(x) = \langle\hat{\boldsymbol{E}}^-(x)\hat{\boldsymbol{E}}^+(x)\rangle$ at $x = (\boldsymbol{r},\omega)$, where $\boldsymbol{r}$ is a position outside the material and the scattering frequency ω differs from the pump frequency $\omega_{\rm in}$. The two-photon coincidence intensity is evaluated by the second-order correlation $C^{(2)}(x_1,x_2) = \langle\hat{\boldsymbol{E}}^-(x_1)\hat{\boldsymbol{E}}^-(x_2)\hat{\boldsymbol{E}}^+(x_2)\hat{\boldsymbol{E}}^+(x_1)\rangle = C^{(2)}_S(x_1,x_2) + C^{(2)}_N(x_1,x_2)$. Here, $C^{(2)}_S(x_1,x_2)$ is the intensity of correlated photons satisfying the frequency conservation $2\omega_{\rm in} = \omega_1 + \omega_2$, while $C^{(2)}_N(x_1,x_2) = C^{(1)}(x_1)C^{(1)}(x_2)$ is the intensity of accidental pairs and is written as a product of two first-order correlations [15].

We consider a CuCl film with thickness d, and the z-axis is perpendicular to its surface. We consider only the lowest relative motion of excitons and biexcitons and assume sinusoidal wavefunctions for their center-of-mass motion (indexed by n) as seen in Fig. 1(b). We assume their standard parabolic energy dispersions and follow Ref. 16 for other excitonic parameters. Concerning biexcitons, its translational mass is $m_{\rm bx} = 2.3m_{\rm ex}$, and the binding energy is $\Delta_{\rm bx} = 32.2$ meV [8]. From Ref. 17, we consider the effective volume as $|\Phi|^2 = 80$ nm^3 and the damping rate as $\gamma_{\rm bx} = 13.2$ μeV. The pumping light is a continuous plane wave perpendicular to the film, and has the same frequency as the giant two-photon absorption of CuCl except in Fig. 2(b), where $\omega_{\rm in}$ is tuned to resonantly excite $n = 6$ biexciton state. In both cases, $\hbar\omega_{\rm in} \simeq \hbar\omega_{\rm T} - \Delta_{\rm bx}/2$, where $\hbar\omega_{\rm T} = 3.2022$ eV is the transverse bare exciton energy. We consider the pump power as $I = 10$ μW (except in Fig. 3(b)) as used in Ref. 6, while spectral shapes of the RHPS are not modified by changing I. The scattering angle θ is defined as providing the in-plane wavenumber $k_\parallel = (\omega_{\rm T}/c)\sin\theta$, and the above correlation functions are transformed into $k_\parallel$-space as $x = (\theta, z, \omega)$, while they depend on z only for whether the scattering fields are forward or backward with respect to the pump propagation. We define the horizontal (H) and vertical (V) directions of the polarization with respect to the scattering plane.

Fig. 2 shows the polarization-resolved spectra of forward scattering intensity (proportional to $C^{(1)}$ [18]) at thicknesses of (a) 7 μm and (b) 200 nm. The nonradiative damping rate of excitons is $\gamma_{\rm ex} = 0.5$ meV and the scattering angle is $\theta = 60°$. In the case of the bulk-like thickness [Fig. 2(a)], the four peaks, namely, $\mathrm{M_L}$, $\mathrm{M_T}$, LEP, and HEP (lower and higher energy polariton) are reproduced as observed in experiments [5, 6, 8]. The LEP and HEP correspond to the RHPS process, while $\mathrm{M_T}$ and $\mathrm{M_L}$ are caused by the biexciton relaxation to the transverse and longitudinal excitons, respectively. The frequencies of LEP and HEP depend on scattering angle under the conservation of energy and wavevector in bulk materials. Decreasing the film thickness, the LEP and HEP peaks diminish due to the relax of the wavevector conservation. Instead, multiple peaks appear in the

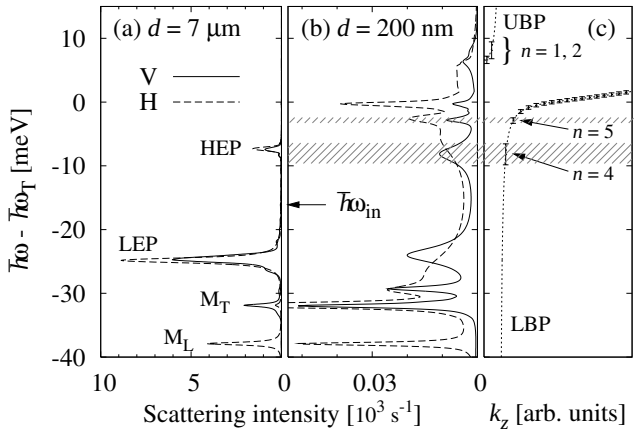

FIG. 2: Forward RHPS spectra of CuCl film with thicknesses of (a) $d = 7$ μm and (b) $d = 200$ nm. V- and H-polarized spectra are plotted by solid and dashed lines, respectively. (c) Dotted lines represent the dispersion curves of upper and lower branch polaritons (UBP and LBP), and vertical bars indicate the resonance frequency of V-polarized exciton-photon coupled modes in the film with $d = 200$ nm. The length of the bars represents the sum of radiative and nonradiative decay rates of the coupled modes. n denotes the index of the original exciton state of each coupled mode. Parameters: $\gamma_{\rm ex} = 0.5$ meV, $\theta = 60°$.

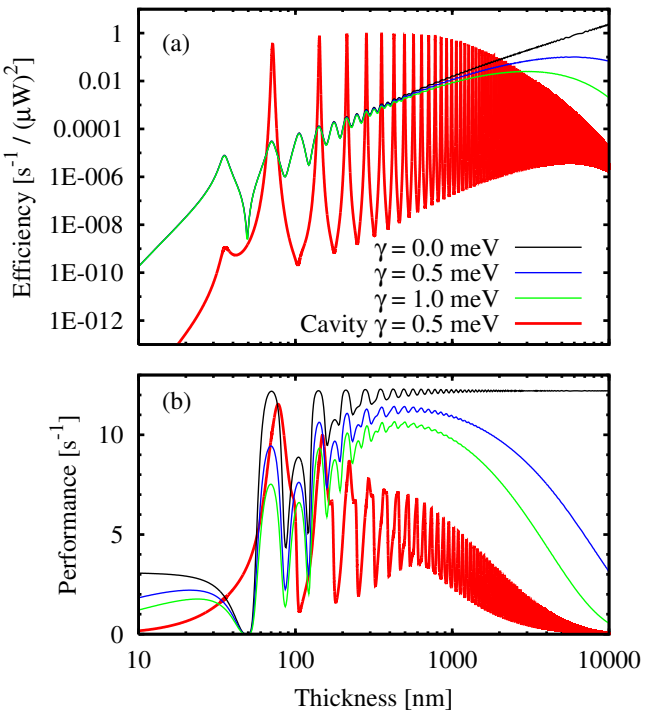

FIG. 3: Thickness dependence of (a) generation efficiency S/I^2 and (b) performance P. Dielectric constant of outside is $\varepsilon_{\rm bg}$, scattering frequencies are the same as that of pumping field, and scattering is forward with $\theta = 0°$ (black, blue, and green). The red lines represent backward emission from a CuCl film with an optical cavity, whose mode frequency is tuned to $\omega_{\rm T}$.

LEP-HEP frequency region as seen in Fig. 2(b). These anomalous peaks can be interpreted by the energy level structure of exciton-photon coupled modes in the nano film [9–11, 16], which are shown in Fig. 2(c) as vertical bars with length of sum of the radiative and nonradiative damping rates. The scattering spectra reflect the anomalous level structure of the coupled modes, because a biexciton relaxes into a coupled mode by emitting a photon (a peak on the lower energy side) with satisfying the energy conservation. It is worth noting that we can significantly modify resonance frequencies and radiative lifetimes of the exciton-photon coupled modes by designing the material structure, i.e., material shape, size, arrangement, and external environments [9, 11, 16]. Since the anomalous level structures depend even on propagation angle and polarization direction, the nano-structured materials have much degrees of freedom to control the frequencies, angles, polarizations and phase difference of generated entangled state. This aspect is essentially different from the cases of bulk crystals [1, 5, 6] and of the single quantum dot systems [2, 3].

For the high-power generation of the entangled photons, the important factors are the generation efficiency and also the statistical accuracy, i.e., the amount of accidental pairs. For a pumping beam with power I, the signal intensity $S \propto C_S^{(2)}$ (amount of correlated pairs) is proportional to I^2, while the noise intensity $N \propto C_N^{(2)}$ (amount of accidental pairs) is proportional to I^4, because an accidental pair is involved with two biexcitons. This implies that, by increasing the pump power I, the S/N ratio decreases in contrast to the increase of S [6]. Here, we introduce another measure termed "performance" P defined as signal intensity S under a certain S/N ratio (I is tuned to give this ratio). This quantity does not depend on I, and represents the material potential for generating strong and qualified entangled-photon beams. While we suppose $S/N = 20$ as reported in Ref. 6 to calculate $P = S^2/20N$, the spectral shape of the performance does not depend on a chosen S/N ratio.

Fig. 3 shows thickness dependences of (a) generation efficiency S/I^2 and (b) performance P. For simplicity, we suppose that the two scattering fields are perpendicular to the film ($\theta = 0°$) and frequencies are $\omega_{1/2} = \omega_{\rm in} \pm 0^+$. The black, blue, and green lines ($\gamma_{\rm ex} = 0$, 0.5, and 1.0 meV, respectively) represent the forward emission from a CuCl film existing in a dielectric medium with $\varepsilon_{\rm bg}$. As seen in Fig. 3(a) and also in Ref. 13, the thickness maximizing the generation efficiency is changed by $\gamma_{\rm ex}$, and it is in the order of micrometers or more for CuCl crystals.

However, as seen in Fig. 3(b), the performance decreases with increasing thickness for non-zero $\gamma_{\rm ex}$ at thickness range of micrometers, because the amplitudes

of scattering fields decrease during the propagation in the absorptive film (see Fig. 1(a)), and the performance does not increase even if $\gamma_{\rm ex} = 0$. The maximum performance in Fig. 3(b) is the ideal quantity, and it only depends on measurement conditions, such as resolutions of angle and frequency, but not on material parameters [18]. Therefore, the generation efficiency (generation probability for one pump pulse) is limited by the statistical accuracy (S/N ratio) when we use bulk crystals [6]. However, at thickness of from 50 nm to 1000 nm, it is worth noting that nearly ideal performance values can be obtained at particular thicknesses even if $\gamma_{\rm ex}$ is non-zero. This is because the radiative decay is dominant in such nano films owing to the exciton superradiance [9, 16], and the entangled pairs can go outside the film without decreasing the amplitude. Therefore, nano films generally show a high performance, and this rapid decay is also desired for the high repetition excitation, which also recovers the signal intensity with keeping the S/N ratio [6]. A good performance is obtained only when the resonance energy of exciton-photon coupled mode is just equal to a half of the biexciton energy. This condition appears as an oscillatory behavior in this crossover thickness region, because the center-of-mass of biexcitons is confined and the energy levels of coupled modes are modified by changing the thickness.

However, as seen in Fig. 3(a), the generation efficiency of nano films is much lower than that of bulk crystals. In other words, a strong pump power is required to achieve a sufficient signal intensity at the thickness range of nanometers. This problem can be overcome by controlling the light-matter coupling by using an optical cavity. Avoiding essential modifications of the biexciton level scheme and considering an existing sample, we treat a cavity with a low quality factor (Q-factor) as reported in the experiment [19], namely a CuCl film in a distributed Bragg reflector (DBR) cavity composed by PbF_2 and $PbBr_2$. The DBR reflectors are considered by the background dielectric function $\varepsilon_{\rm bg}(\boldsymbol{r}, \omega)$. The red lines in Fig. 3 represent the backward emission from the cavity structure, where the cavity mode frequency is tuned to $\omega_{\rm T}$, $\gamma_{\rm ex} = 0.5$ meV, and the periods of the incident- and transmitted-side are 4 and 16, respectively. This system corresponds to the weak bipolariton regime, where the energy splitting between polariton and biexciton levels are small compared to their broadening. This situation is in contrast with Ref. 20, where the strong enhancement of entangled-photon generation from a quantum well in a cavity with higher Q-factor has been discussed based on the biexcitonic cavity-QED picture or the strong bipolariton picture. As seen in Fig. 3(a), since the biexcitons are effectively created, the generation efficiency is significantly enhanced at thickness of nanometers, and it is larger than the maximum value in the previous situation ($\gamma_{\rm ex} = 0.5$ meV, blue line). The enhancement also occurs when the energy of polariton (exciton-photon coupled mode) is equal to a half of biexciton energy, which is consistent with Ref. 20. Comparing to the previous data (blue line), the period of the oscillation is doubled, because the RHPS process involving biexcitons with odd-parity center-of-mass motion is forbidden in an one-sided optical cavity. On the other hand, as seen in Fig. 3(b), at thickness of micrometers, the performance is suppressed compared to that by the bare CuCl film. This is because of the multiple reflection inside the cavity, and the scattered fields nonradiatively decay during the propagation. In contrast, at thickness of nanometers, especially at 80 nm, the performance almost keeps the ideal quantity, because of the enhancement of excitons' radiative decay rate by the optical cavity or the exciton superradiance [9, 16]. In this way, for the optimum condition, we can highly control both the generation efficiency and the performance by manipulating the confinement of biexcitons and the level structure of the exciton-photon coupled modes in a nano film embedded in an optical cavity.

In summary, semiconductor nano-films have much degrees of freedom to control generated states of entangled photon pairs. They show a high performance from the viewpoint of statistical accuracy, and the trade-off problem in bulk materials can be overcome by the enhancement of radiative decay of excitons. By using a cavity under the weak bipolariton regime, the generation efficiency can be enhanced with keeping the high performance. We believe that our results make a breakthrough of entangled-photon generation with both a high generation efficiency and the ideal statistical accuracy.

The authors thank K. Edamatsu, G. Oohata, H. Ajiki, and H. Oka for their helpful discussions. This work was partially supported by the Japan Society for the Promotion of Science (JSPS); a Grant-in-Aid for Creative Science Research, 17GS1204, 2005; and a Grant-in-Aid for JSPS Research Fellows.

SUPPLEMENTARY MATERIAL

Hamiltonian

We consider the Hamiltonian on the main paper as

$$H = H_{\rm ex} + H_{\rm res} + H_{\rm int} + H_{\rm em}, \tag{A.1}$$

where $H_{\rm ex}$ describes the excitonic systems, $H_{\rm res}$ represents a reservoir for the nonradiative damping of excitons, $H_{\rm int}$ is the exciton-photon interaction, and $H_{\rm em}$ describes the electromagnetic fields and a background dielectric medium, which is the Hamiltonian discussed by Suttorp et al. in Ref. [21] and also used in Ref. [12]. We consider the Hamiltonian of excitonic system as

$$H_{\rm ex} = \sum_{\mu} \hbar\omega_{\mu} b_{\mu}^{\dagger} b_{\mu} + \frac{1}{2} \sum_{\mu,\mu',\nu,\nu'} V_{\mu,\nu;\mu',\nu'} b_{\mu}^{\dagger} b_{\nu}^{\dagger} b_{\nu'} b_{\mu'}, \tag{A.2}$$

where b_μ is the annihilation operator of an exciton in state μ and ω_μ is its eigenfrequency. We treat the excitons as pure bosons satisfying

$$\left[b_\mu, b^\dagger_{\mu'}\right] = \delta_{\mu,\mu'}, \tag{A.3a}$$

$$[b_\mu, b_{\mu'}] = 0, \tag{A.3b}$$

and their non-bosonic behavior is described by the exciton-exciton interaction, the second term in Eq. (A.2). The reservoir $H_{\rm res}$ is written as

$$H_{\rm res} = \sum_\mu \int_0^\infty \mathrm{d}\Omega \, \big\{\hbar\Omega d^\dagger_\mu(\Omega) d_\mu(\Omega) + \left[b_\mu + b^\dagger_\mu\right]\left[g_\mu(\Omega) d_\mu(\Omega) + g^*_\mu(\Omega) d^\dagger_\mu(\Omega)\right]\big\}, \tag{A.4}$$

where $d_\mu(\Omega)$ is the annihilation operator of harmonic oscillator with frequency Ω interacting with excitons in state μ, and $g_\mu(\Omega)$ is the coupling coefficient. The oscillators are independent with each other and satisfy the following commutation relations:

$$[d_\mu(\Omega), d^\dagger_{\mu'}(\Omega')] = \delta_{\mu,\mu'}\delta(\Omega - \Omega'), \tag{A.5a}$$

$$[d_\mu(\Omega), d_{\mu'}(\Omega')] = 0. \tag{A.5b}$$

Further, $H_{\rm int}$ is simply written as a product of electric field $\boldsymbol{E}(\boldsymbol{r})$ and excitonic polarization $\boldsymbol{P}_{\rm ex}(\boldsymbol{r})$:

$$H_{\rm int} = -\int \mathrm{d}\boldsymbol{r} \; \boldsymbol{P}_{\rm ex}(\boldsymbol{r}) \cdot \boldsymbol{E}(\boldsymbol{r}). \tag{A.6}$$

Here, the excitonic polarization is represented as

$$\boldsymbol{P}_{\rm ex}(\boldsymbol{r}) = \sum_\mu \boldsymbol{\mathcal{P}}_\mu(\boldsymbol{r}) b_\mu + \mathrm{H.c.}, \tag{A.7}$$

where the coefficient $\boldsymbol{\mathcal{P}}_\mu(\boldsymbol{r})$ is represented by the exciton center-of-mass wavefunction $g_\mu(\boldsymbol{r})$ and unit vector $\boldsymbol{e}_\mu$ of polarization direction as

$$\boldsymbol{\mathcal{P}}_\mu(\boldsymbol{r}) = M \boldsymbol{e}_\mu g_\mu(\boldsymbol{r}). \tag{A.8}$$

The absolute value of M can be estimated by the longitudinal-transverse (LT) splitting energy $\Delta_{\rm LT} = |M|^2/\varepsilon_0\varepsilon_{\rm bg}$ of excitons and by background dielectric constant $\varepsilon_{\rm bg}$ of excitonic medium.

Equation of motion

According to Ref. [12] or the QED theories of dispersive and absorbing media [21–23], the equation of motion of the electric field is derived in frequency domain as

$$\boldsymbol{\nabla}\times\boldsymbol{\nabla}\times\hat{\boldsymbol{E}}^+(\boldsymbol{r},\omega) - \frac{\omega^2}{c^2}\varepsilon_{\rm bg}(\boldsymbol{r},\omega)\hat{\boldsymbol{E}}^+(\boldsymbol{r},\omega) = \mathrm{i}\mu_0\omega\hat{\boldsymbol{J}}_0(\boldsymbol{r},\omega) + \mu_0\omega^2\hat{\boldsymbol{P}}^+_{\rm ex}(\boldsymbol{r},\omega). \tag{A.9}$$

Here, $\varepsilon_{\rm bg}(\boldsymbol{r},\omega)$ is the dielectric function of the background medium. $\hat{\boldsymbol{J}}_0(\boldsymbol{r},\omega)$ describes the fluctuation of electromagnetic fields and satisfies

$$\left[\hat{\boldsymbol{J}}_0(\boldsymbol{r},\omega), \{\hat{\boldsymbol{J}}_0(\boldsymbol{r}',\omega'^*)\}^\dagger\right] = \left[\hat{\boldsymbol{J}}_0(\boldsymbol{r},\omega), \hat{\boldsymbol{J}}_0(\boldsymbol{r}',-\omega')\right] = \delta(\omega-\omega')\delta(\boldsymbol{r}-\boldsymbol{r}')\frac{\varepsilon_0\hbar\omega^2}{\pi}\mathrm{Im}[\varepsilon_{\rm bg}(\boldsymbol{r},\omega)]\mathbf{1}. \tag{A.10}$$

In the same manner as in Ref. [12], under the rotating-wave approximation (RWA), we obtain the equation of excitons' motion in frequency domain as

$$[\hbar\omega_\mu - \hbar\omega - \mathrm{i}\gamma_{\rm ex}/2]\,\hat{b}_\mu(\omega) = \int \mathrm{d}\boldsymbol{r} \; \boldsymbol{\mathcal{P}}^*_\mu(\boldsymbol{r})\cdot\hat{\boldsymbol{E}}^+(\boldsymbol{r},\omega) + \hat{\mathcal{D}}_\mu(\omega) - \sum_\nu\sum_{\mu',\nu'} V_{\mu,\nu;\mu',\nu'}\int_{-\infty}^\infty \mathrm{d}t \; \frac{\mathrm{e}^{\mathrm{i}\omega t}}{2\pi} b^\dagger_\nu(t) b_{\nu'}(t) b_{\mu'}(t), \tag{A.11}$$

where $\gamma_{\rm ex}$ is the nonradiative damping width (defined by $\{g_\mu(\Omega)\}$ in Eq. (D7) of Ref. [12]), and $\hat{\mathcal{D}}_\mu(\omega)$ is the fluctuation operator satisfying

$$\left[\hat{\mathcal{D}}_\mu(\omega), \{\hat{\mathcal{D}}_{\mu'}(\omega'^*)\}^\dagger\right] = \left[\hat{\mathcal{D}}_\mu(\omega), \hat{\mathcal{D}}_{\mu'}(-\omega')\right] = \delta_{\mu,\mu'}\delta(\omega-\omega')\frac{\hbar\gamma_{\rm ex}}{2\pi}. \tag{A.12}$$

The last term on the right hand side of Eq. (A.11) is the nonlinear term due to the exciton-exciton interaction.

Here, we define a new operator

$$B_\lambda \equiv \frac{1}{2}\sum_{\mu,\nu} F^*_{\lambda,\mu,\nu} b_\nu b_\mu, \tag{A.13}$$

which annihilates a biexciton (two excitons) in state λ or describes a two-exciton eigen state $B^\dagger_\lambda|\mathrm{g}\rangle$ by applying it to the matter ground state $|\mathrm{g}\rangle$. The coefficient $F_{\lambda,\mu,\nu}$ is invariant by the exchange of two exciton indices as

$$F_{\lambda,\mu,\nu} = F_{\lambda,\nu,\mu}. \tag{A.14}$$

Further, it is ortho-normal as

$$\frac{1}{2}\sum_{\mu,\nu} F_{\lambda,\mu,\nu}F^*_{\lambda',\mu,\nu} = \delta_{\lambda,\lambda'}, \tag{A.15}$$

and also has a completeness

$$\sum_\lambda F_{\lambda,\mu,\nu}F^*_{\lambda,\mu',\nu'} = \delta_{\mu,\mu'}\delta_{\nu,\nu'} + \delta_{\mu,\nu'}\delta_{\nu,\mu'}. \tag{A.16}$$

From the excitonic Hamiltonian (A.2), the coefficient $F_{\lambda,\mu,\nu}$ and eigen frequency Ω_λ of biexciton eigen state λ should satisfy

$$(\hbar\omega_\mu + \hbar\omega_\nu)F_{\lambda,\mu,\nu} + \sum_{\mu',\nu'} V_{\mu,\nu;\mu',\nu'}F_{\lambda,\mu',\nu'} = \hbar\Omega_\lambda F_{\lambda,\mu,\nu}. \tag{A.17}$$

By using Eqs. (A.14) and (A.16), we can rewrite Eq. (A.13) as

$$\sum_{\lambda} F_{\lambda,\mu,\nu} B_\lambda = b_\nu b_\mu. \tag{A.18}$$

Therefore, from this relation and Eq. (A.17), we can rewrite Eq. (A.11) as

$$\begin{aligned}
&[\hbar\omega_\mu - \hbar\omega - \mathrm{i}\gamma_{\mathrm{ex}}/2]\,\hat{b}_\mu(\omega) \\
&= \int \mathrm{d}\boldsymbol{r}\ \boldsymbol{\mathcal{P}}^*_\mu(\boldsymbol{r})\cdot\hat{\boldsymbol{E}}^+(\boldsymbol{r},\omega) + \hat{\mathcal{D}}_\mu(\omega) \\
&\quad + \sum_{\lambda,\nu}(\hbar\omega_\mu + \hbar\omega_\nu - \hbar\Omega_\lambda)F_{\lambda,\mu,\nu} \\
&\quad \times \int_{-\infty}^{\infty} \mathrm{d}\omega'\ \{\hat{b}_\nu(\omega'-\omega)\}^\dagger \hat{B}_\lambda(\omega').
\end{aligned} \tag{A.19}$$

On the other hand, the equation of motion of B_λ is derived in frequency domain as

$$\begin{aligned}
&(\hbar\Omega_\lambda - \hbar\omega)\hat{B}_\lambda(\omega) \\
&= \sum_{\mu,\nu} F^*_{\lambda,\mu,\nu} \int_{-\infty}^{\infty} \mathrm{d}\omega'\ (\hbar\omega_\nu - \hbar\omega')\hat{b}_\nu(\omega')\hat{b}_\mu(\omega-\omega').
\end{aligned} \tag{A.20}$$

In principle, the biexciton-resonant hyperparametric scattering (RHPS) process is described by equations of motion (A.9), (A.19), and (A.20), and commutation relations (A.10) and (A.12). However, in the actual calculation, we use the following approximation.

Approximation for RHPS process

We suppose that a coherent light beam resonantly excites biexcitons and their amplitude is large enough compared to the vacuum fluctuation. In this case, if we do not consider the other higher processes, the biexciton operator in the nonlinear term of Eq. (A.19) can be replaced by its amplitude $\mathcal{B}_\lambda(\omega') = \langle \hat{B}_\lambda(\omega')\rangle$. Further, we replace $\hat{b}_\nu(\omega'-\omega)$ in the nonlinear term by $\hat{b}^{(1)}_\nu(\omega'-\omega)$, which satisfies the linear equation

$$\begin{aligned}
&[\hbar\omega_\mu - \hbar\omega - \mathrm{i}\gamma_{\mathrm{ex}}/2]\,\hat{b}^{(1)}_\mu(\omega) \\
&= \int \mathrm{d}\boldsymbol{r}\ \boldsymbol{\mathcal{P}}^*_\mu(\boldsymbol{r})\cdot\hat{\boldsymbol{E}}^+(\boldsymbol{r},\omega) + \hat{\mathcal{D}}_\mu(\omega).
\end{aligned} \tag{A.21}$$

Simultaneously solving this equation and Eq. (A.9), $\hat{b}^{(1)}_\mu(\omega)$ can be expressed by the fluctuation operators $\hat{\boldsymbol{J}}_0(\boldsymbol{r},\omega)$ and $\hat{\mathcal{D}}_\mu(\omega)$. Under the above approximation, we simultaneously solve Eq. (A.9) and

$$\begin{aligned}
&[\hbar\omega_\mu - \hbar\omega - \mathrm{i}\gamma_{\mathrm{ex}}/2]\,\hat{b}_\mu(\omega) \\
&\simeq \int \mathrm{d}\boldsymbol{r}\ \boldsymbol{\mathcal{P}}^*_\mu(\boldsymbol{r})\cdot\hat{\boldsymbol{E}}^+(\boldsymbol{r},\omega) + \hat{\mathcal{D}}_\mu(\omega) \\
&\quad + \sum_{\lambda,\nu}(\hbar\omega_\mu + \hbar\omega_\nu - \hbar\Omega_\lambda)F_{\lambda,\mu,\nu} \\
&\quad \times \int_{-\infty}^{\infty} \mathrm{d}\omega'\ \{\hat{b}^{(1)}_\nu(\omega'-\omega)\}^\dagger \mathcal{B}_\lambda(\omega'),
\end{aligned} \tag{A.22}$$

and then represent $\hat{\boldsymbol{E}}^+(\boldsymbol{r},\omega)$ by the fluctuation operators $\hat{\boldsymbol{J}}_0(\boldsymbol{r},\omega)$ and $\hat{\mathcal{D}}_\mu(\omega)$. The calculation procedure is straightforward by using the Green's function technique (see section or Ref. [12]).

For the calculation of $\mathcal{B}_\lambda(\omega)$, we suppose that the biexciton amplitude does not decrease by the RHPS process, because its contribution is small compared to the incident light. Under this approximation, by phenomenologically introducing a damping constant γ_{bx}, the biexciton amplitude is obtained from Eq. (A.20) as

$$\begin{aligned}
\langle \hat{B}_\lambda(\omega)\rangle &\simeq \frac{1}{\hbar\Omega_\lambda - \hbar\omega - \mathrm{i}\gamma_{\mathrm{bx}}/2}\sum_{\mu,\nu} F^*_{\lambda,\mu,\nu} \\
&\quad \times \int_{-\infty}^{\infty} \mathrm{d}\omega'\ (\hbar\omega_\nu - \hbar\omega')\langle \hat{b}^{(1)}_\nu(\omega')\rangle\langle \hat{b}^{(1)}_\mu(\omega-\omega')\rangle,
\end{aligned} \tag{A.23}$$

where $\langle \hat{b}^{(1)}_\nu(\omega')\rangle$ can be calculated from Eqs. (A.9) and (A.21) by considering an incident light beam as a homogeneous solution of Eq. (A.9). Under the weak bipolariton regime, where the coupling between polariton and biexciton is small enough compared to their broadening, the approximated expression (A.23) of biexciton amplitude is sufficient for the discussion of RHPS process.

Model of biexcitons

Although $F_{\lambda,\mu,\nu}$ and Ω_λ should be determined from (A.17) for given nonlinear coefficient $V_{\mu,\nu;\mu',\nu'}$ in principle, we instead suppose them from the experimental results. This treatment is useful because we already know many parameters of the lowest biexciton level in CuCl by the longstanding experimental and theoretical studies [8].

It is well known that the lowest level of biexciton in CuCl is singlet and has zero angular momentum because of the exchange interaction between two electrons and between two holes [8]. Since we suppose the resonant excitation of the lowest level, we only consider the lowest relative motion of biexciton. Further, according to the RHPS experiments in Ref. 24, the lowest biexciton state mainly consists of $1s$ excitons, and the contribution from the higher exciton states was estimated in the order of 10^{-4}. Therefore, we consider only $1s$ relative motion of

excitons, which has a degree of freedom of polarization direction $\xi_\mu = \{x, y, z\}$. The coefficient $F_{\lambda,\mu,\nu}$ is proportional to the polarization selection rule as

$$\delta_{\lambda,\mu,\nu} = \delta_{\xi_\mu,\xi_\nu}. \tag{A.24}$$

Considering the relative motion $\Psi(\boldsymbol{r})$ of two excitons in the lowest biexciton level, the coefficient is written as

$$F_{\lambda,\mu,\nu} = \delta_{\lambda,\mu,\nu} \int \mathrm{d}\boldsymbol{r} \int \mathrm{d}\boldsymbol{r}'\ \Psi(\boldsymbol{r}') G_\lambda(\boldsymbol{r}) g^*_\mu(\boldsymbol{r}+\boldsymbol{r}') g^*_\nu(\boldsymbol{r}), \tag{A.25}$$

where $g_m(\boldsymbol{r})$ and $G_l(\boldsymbol{r})$ are center-of-mass wavefunctions of excitons and biexcitons, respectively. Here, we suppose that the Bohr radius of biexciton is much smaller than the crystal size, and then we approximate the above expression as

$$F_\lambda \simeq \delta_{\lambda,\mu,\nu} \Phi \int \mathrm{d}\boldsymbol{r}\ G_\lambda(\boldsymbol{r})\ g^*_\mu(\boldsymbol{r})\ g^*_\nu(\boldsymbol{r}), \tag{A.26}$$

where Φ is defined as

$$\Phi \equiv \int \mathrm{d}\boldsymbol{r}\ \Psi(\boldsymbol{r}), \tag{A.27}$$

and $|\Phi|^2$ represents the effective volume of the lowest biexciton state. Therefore, we can separately consider the relative and center-of-mass motions of biexcitons. $|\Phi|^2$ has been estimated by an experiment [17], and was also used as a parameter in calculation [25].

Observables

For the one-photon scattering intensity at $\boldsymbol{r}$ with polarization direction $\boldsymbol{e}$ and frequency ω (not equal to pump frequency ω_{in}), its intensity is proportional to the first-order correlation function

$$C^{(1)}(\boldsymbol{r}, \boldsymbol{e}, \omega) = \boldsymbol{e} \cdot \langle \hat{\boldsymbol{E}}^-(\boldsymbol{r}, \omega) \hat{\boldsymbol{E}}^+(\boldsymbol{r}, \omega) \rangle \cdot \boldsymbol{e}. \tag{A.28}$$

This function can be calculated by the commutation relations (A.10) and (A.12). The two-photon coincidence intensity between $(\boldsymbol{r}_1, \boldsymbol{e}_1, \omega_1)$ and $(\boldsymbol{r}_2, \boldsymbol{e}_2, \omega_2)$ is proportional to the second-order correlation function

$$\begin{aligned} C^{(2)}(\boldsymbol{r}_1, \boldsymbol{e}_1, \omega_1; \boldsymbol{r}_2, \boldsymbol{e}_2, \omega_2) &= \langle \boldsymbol{e}_1 \cdot \hat{\boldsymbol{E}}^-(\boldsymbol{r}_1, \omega_1) \boldsymbol{e}_2 \cdot \hat{\boldsymbol{E}}^-(\boldsymbol{r}_2, \omega_2) \boldsymbol{e}_2 \cdot \hat{\boldsymbol{E}}^+(\boldsymbol{r}_2, \omega_2) \boldsymbol{e}_1 \cdot \hat{\boldsymbol{E}}^+(\boldsymbol{r}_1, \omega_1) \rangle \\ &= C^{(2)}_S(\boldsymbol{r}_1, \boldsymbol{e}_1, \omega_1; \boldsymbol{r}_2, \boldsymbol{e}_2, \omega_2) + C^{(2)}_N(\boldsymbol{r}_1, \boldsymbol{e}_1, \omega_1; \boldsymbol{r}_2, \boldsymbol{e}_2, \omega_2), \end{aligned} \tag{A.29}$$

where we neglect the interference term that appears only under $\omega_1 = \omega_2$. $C^{(2)}_S$ represents the signal intensity or the number of correlated photon pairs, which satisfies the energy conservation $\omega_1 + \omega_2 = 2\omega_{\mathrm{in}}$. On the other hand, $C^{(2)}_N$ appears for arbitrary pair of ω_1 and ω_2. This represents the accidental coincidence of emitted photons from independent biexcitons, because it is just the product of two first-order correlation functions

$$\begin{aligned} &C^{(2)}_N(\boldsymbol{r}_1, \boldsymbol{e}_1, \omega_1; \boldsymbol{r}_2, \boldsymbol{e}_2, \omega_2) \\ &\equiv C^{(1)}(\boldsymbol{r}_1, \boldsymbol{e}_1, \omega_1) C^{(1)}(\boldsymbol{r}_2, \boldsymbol{e}_2, \omega_2). \end{aligned} \tag{A.30}$$

Solving wave equation

Here, we explain how we simultaneously solve Eq. (A.9) and equation of exciton motion. By using the dyadic Green's function satisfying

$$\boldsymbol{\nabla} \times \boldsymbol{\nabla} \times \mathbf{G}(\boldsymbol{r}, \boldsymbol{r}', \omega) - \frac{\omega^2}{c^2} \varepsilon_{\mathrm{bg}}(\boldsymbol{r}, \omega) \mathbf{G}(\boldsymbol{r}, \boldsymbol{r}', \omega) = \delta(\boldsymbol{r} - \boldsymbol{r}') \mathbf{1}, \tag{A.31}$$

we can rewrite Eq. (A.9) as

$$\hat{\boldsymbol{E}}^+(\boldsymbol{r}, \omega) = \hat{\boldsymbol{E}}^+_0(\boldsymbol{r}, \omega) + \mu_0 \omega^2 \int \mathrm{d}\boldsymbol{r}'\ \mathbf{G}(\boldsymbol{r}, \boldsymbol{r}', \omega) \cdot \hat{\boldsymbol{P}}^+_{\mathrm{ex}}(\boldsymbol{r}', \omega), \tag{A.32}$$

where $\hat{\boldsymbol{E}}^+_0(\boldsymbol{r}, \omega)$ is the electric field in the background (H_{em}) system, and it is defined as

$$\hat{\boldsymbol{E}}^+_0(\boldsymbol{r}, \omega) \equiv \mathrm{i}\mu_0 \omega \int \mathrm{d}\boldsymbol{r}'\ \mathbf{G}(\boldsymbol{r}, \boldsymbol{r}', \omega) \cdot \hat{\boldsymbol{J}}_0(\boldsymbol{r}', \omega). \tag{A.33}$$

Further, from Eq. (A.10), $\hat{\boldsymbol{E}}^+_0(\boldsymbol{r}, \omega)$ satisfies [12]

$$\begin{aligned} &\left[\hat{\boldsymbol{E}}^+_0(\boldsymbol{r}, \omega), \hat{\boldsymbol{E}}^-_0(\boldsymbol{r}', \omega')\right] = \left[\hat{\boldsymbol{E}}^+_0(\boldsymbol{r}, \omega), \hat{\boldsymbol{E}}^+_0(\boldsymbol{r}', -\omega')\right] \\ &= \delta(\omega - \omega') \frac{\mu_0 \hbar \omega^2}{\mathrm{i}2\pi} [\mathbf{G}(\boldsymbol{r}, \boldsymbol{r}', \omega) - \mathbf{G}^*(\boldsymbol{r}, \boldsymbol{r}', \omega)]. \end{aligned} \tag{A.34}$$

The expression of $\mathbf{G}(\boldsymbol{r}, \boldsymbol{r}', \omega)$ in planar system (dielectric multi-layer) is already known [26].

Substituting Eq. (A.32) into Eq. (A.22), we obtain the

equation set for exciton operators as

$$\sum_{\mu'} S_{\mu,\mu'}(\omega)\hat{b}_{\mu'}(\omega) = \int \mathrm{d}\boldsymbol{r}\ \boldsymbol{\mathcal{P}}^*_\mu(\boldsymbol{r})\cdot\hat{\boldsymbol{E}}^+_0(\boldsymbol{r},\omega) + \hat{\mathcal{D}}_\mu(\omega) + \sum_{\lambda,\nu}(\hbar\omega_\mu + \hbar\omega_\nu - \hbar\Omega_\lambda)F_{\lambda,\mu,\nu} \times \int_{-\infty}^{\infty}\mathrm{d}\omega'\ \{\hat{b}^{(1)}_\nu(\omega'-\omega)\}^\dagger\mathcal{B}_\lambda(\omega'), \tag{A.35}$$

where the coefficient in the left-hand side is defined as

$$S_{\mu,\mu'}(\omega) \equiv [\hbar\omega_\mu - \hbar\omega - \mathrm{i}\gamma_{\mathrm{ex}}/2]\,\delta_{\mu,\mu'} - \mu_0\omega^2\int\mathrm{d}\boldsymbol{r}\int\mathrm{d}\boldsymbol{r}'\ \boldsymbol{\mathcal{P}}^*_\mu(\boldsymbol{r})\cdot\mathbf{G}(\boldsymbol{r},\boldsymbol{r}',\omega)\cdot\boldsymbol{\mathcal{P}}_{\mu'}(\boldsymbol{r}'). \tag{A.36}$$

The last term of Eq. (A.36) is the renormalization due to the exciton-exciton interaction via the electromagnetic fields. Further, the equation of operator $\hat{b}^{(1)}_\mu(\omega)$ in the linear regime is also rewritten as

$$\sum_{\mu'} S_{\mu,\mu'}(\omega)\hat{b}^{(1)}_{\mu'}(\omega) = \int \mathrm{d}\boldsymbol{r}\ \boldsymbol{\mathcal{P}}^*_\mu(\boldsymbol{r})\cdot\hat{\boldsymbol{E}}^+_0(\boldsymbol{r},\omega) + \hat{\mathcal{D}}_\mu(\omega). \tag{A.37}$$

This simultaneous linear equation set is solved by the inverse matrix $\mathbf{W}(\omega) = [\mathbf{S}(\omega)]^{-1}$, and the commutation relation of $\hat{b}^{(1)}_\mu(\omega)$ is derived in Ref. [12] as

$$\left[\hat{b}^{(1)}_\mu(\omega), \{\hat{b}^{(1)}_{\mu'}(\omega'^*)\}^\dagger\right] = \delta(\omega-\omega')\frac{\hbar}{\mathrm{i}2\pi}\left[W_{\mu,\mu'}(\omega) - W^*_{\mu',\mu}(\omega)\right], \tag{A.38a}$$

$$\left[\hat{b}^{(1)}_\mu(\omega), \hat{b}^{(1)}_{\mu'}(-\omega')\right] = 0. \tag{A.38b}$$

Further, Eq. (A.35) is rewritten as

$$\hat{b}_\mu(\omega) \simeq \hat{b}^{(1)}_\mu(\omega) + \sum_{\mu',\lambda,\nu} W_{\mu,\mu'}(\omega)(\hbar\omega_{\mu'} + \hbar\omega_\nu - \hbar\Omega_\lambda) \times F_{\lambda,\mu',\nu}\int_{-\infty}^{\infty}\mathrm{d}\omega'\ \{\hat{b}^{(1)}_\nu(\omega'-\omega)\}^\dagger\mathcal{B}_\lambda(\omega'), \tag{A.39}$$

and then the expression of electric field is obtained by substituting this into Eq. (A.32).

Intensity estimation

We have estimated the scattering intensity, signal S, and noise N of RHPS process from the experimental data in Ref. [6]. For a bulk crystal, the reported maximum count of entangled pairs (sum of HH and VV) is 50 in 300 seconds and the width of the pulse is 2 ns. Since the time resolution is 300 ps [5], the number of pairs in unit time is roughly estimated as

$$\frac{1}{2}\times 50\times\frac{2\ \mathrm{ns}}{300\ \mathrm{ps}}\times\frac{1}{300\ \mathrm{s}} \simeq 0.5\ \mathrm{s}^{-1}. \tag{A.40}$$

The reported signal-to-noise ratio is $S/N = 20$, and then the number of uncorrelated pairs is 0.025 s^{-1}. The reported pump power is $I = 10\ \mu$W. For the intensity estimation of our calculation results, we have suppose that these experimental results correspond to the our data in the case of CuCl film in vacuum with $\gamma_{\mathrm{ex}} = 0.5$ meV and thickness of 7 μm, which is the optimum thickness for the generation efficiency S/I^2. On the main paper, we consider a CuCl film with dielectric medium with $\varepsilon_{\mathrm{bg}}$ or the film with distributed Bragg reflectors.

* Present address: Laboratoire Matériaux et Phénomènes Quantiques, Université Paris Diderot-Paris 7 et CNRS, Case 7021, Bâtiment Condorcet, 75205 Paris Cedex 13, France. E-mail: motoaki.bamba@univ-paris-diderot.fr

[1] P. G. Kwiat, K. Mattle, H. Weinfurter, A. Zeilinger, A. V. Sergienko, and Y. Shih, Phys. Rev. Lett. **75**, 4337 (1995); P. G. Kwiat, E. Waks, A. G. White, I. Appelbaum, and P. H. Eberhard, Phys. Rev. A **60**, R773 (1999).
[2] N. Akopian, N. H. Lindner, E. Poem, Y. Berlatzky, J. Avron, D. Gershoni, B. D. Gerardot, and P. M. Petroff, Phys. Rev. Lett. **96**, 130501 (2006).
[3] R. M. Stevenson, R. J. Young, P. Atkinson, K. Cooper, D. A. Ritchie, and A. J. Shields, Nature **439**, 179 (2006).
[4] Y. Kawabe, H. Fujiwara, R. Okamoto, K. Sasaki, and S. Takeuchi, Opt.Exp. **15**, 14244 (2007).
[5] K. Edamatsu, G. Oohata, R. Shimizu, and T. Itoh, Nature **431**, 167 (2004).
[6] G. Oohata, R. Shimizu, and K. Edamatsu, Phys. Rev. Lett. **98**, 140503 (2007).
[7] T. Itoh and T. Suzuki, J. Phys. Soc. Jpn. **45**, 1939 (1978).
[8] M. Ueta, H. Kanzaki, K. Kobayashi, Y. Toyozawa, and E. Hanamura, *Excitonic Processes in Solids* (Springer, Berlin, 1986).
[9] M. Ichimiya, M. Ashida, H. Yasuda, H. Ishihara, and T. Itoh, Phys. Rev. Lett. **103**, 257401 (2009).
[10] H. Ishihara, J. Kishimoto, and K. Sugihara, Journal of Lumin. **108**, 342 (2004).
[11] A. Syouji, B. P. Zhang, Y. Segawa, J. Kishimoto, H. Ishihara, and K. Cho, Phys. Rev. Lett. **92**, 257401 (2004).
[12] M. Bamba and H. Ishihara, Phys. Rev. B **78**, 085109 (2008).
[13] For example, S. Savasta, G. Martino, and R. Girlanda, Solid State Commun. **111**, 495 (1999).
[14] See the detail on Supplementary Online Material.
[15] While neigther the surface scattering nor the luminescence are not considered in the calculation, accidental pairs mainly come from independent biexcitons [6].
[16] M. Bamba and H. Ishihara, Phys. Rev. B **80**, 125319 (2009).
[17] H. Akiyama, T. Kuga, M. Matsuoka, and M. Kuwata-Gonokami, Phys. Rev. B **42**, 5621 (1990).
[18] We estimate the absolute values of the scattering intensity, generation efficiency, and performance from the experimental values in Ref. 6 [14].
[19] G. Oohata, T. Nishioka, D. Kim, H. Ishihara, and M. Nakayama, Phys. Rev. B **78**, 233304 (2008).
[20] H. Ajiki and H. Ishihara, J. Phys. Soc. Jpn. **76**, 053401 (2007); H. Oka and H. Ishihara, Phys. Rev. Lett. **100**,

170505 (2008).
[21] L. G. Suttorp and M. Wubs, Phys. Rev. A **70**, 013816 (2004).
[22] B. Huttner and S. M. Barnett, Phys. Rev. A **46**, 4306 (1992).
[23] L. Knöll, S. Scheel, and D.-G. Welsch, *QED in Dispersing and Absorbing Dielectric Media*, in *Coherence and Statistics of Photons and Atoms*, edited by J. Peřina,Wiley Series in Lasers and Applications (Wiley, New York, 2001), chapter 1, pp. 1–64, for update, see arXiv:quant-ph/0006121.
[24] E. Tokunaga, A. L. Ivanov, S. V. Nair, and Y. Masumoto, Phys. Rev. B **59**, R7837 (1999).
[25] N. Matsuura and K. Cho, J. Phys. Soc. Jpn. **64**, 651 (1995).
[26] W. C. Chew, *Waves and Fields in Inhomogeneous Media*, IEEE Press Series on Electromagnetic Wave (IEEE, New York, 1995), Reprint edition.